X-Ray Emission and X-Ray Self-Absorption in the High-T_c Superconductor $YBa_2Cu_3O_{6.9}$ and other Copper Oxides

F. Burgäzy, H. Jaeger, K. Schulze, P. Lamparter, and S. Steeb

Max-Planck-Institut für Metallforschung, Institut für Werkstoffwissenschaft, Stuttgart

Z. Naturforsch. **44a**, 180–188 (1989); received December 22, 1988

$O-K_z$ X-ray emission spectra of La_2CuO_4 and $YBa_2Cu_3O_{6.9}$ are compared with calculated spectra. It is shown from $O-K_z$ emission spectra of $YBa_2Cu_3O_x$ with varying oxygen content ($6.0 < x < 6.9$) that with heating the superconducting compound ($x = 6.9$) oxygen atoms are removed from the Cu–O chains. A method for comparing X-ray self-absorption spectra from compounds with different concentrations of the element under consideration is presented. Cu–L self-absorption spectra of $YBa_2Cu_3O_x$ ($6.0 < x < 6.9$) are compared with those of Cu, Cu_2O, CuO, and $NaCuO_2$. By this comparison and from $O-K_z$ emission spectra, oxygen 2p holes are found to be present in the superconducting compound. The ionic character of the Cu–O bonds in the non-superconducting green phase Y_2BaCuO_5 is shown with $O-K_z$ emission and $Cu-L_3$ self-absorption spectroscopy. The energy gap of Y_2BaCuO_5 is found to be about 5 eV.

1. Introduction

In the high-T_c superconductors $La_{2-x}(Ba,Sr)_x CuO_4$ ($x \approx 0.2$) [1, 2] and $YBa_2Cu_3O_x$ ($x \approx 6.9$) [3] the Cu–O-bonding has been explained in different ways:

On one hand, starting with the usual oxygen valency of 2^- simple charge balance considerations lead to the assumption that Cu with valency 3^+ has to be present in these compounds. Several authors indeed found evidence for trivalent copper [4–8 and 12].

On the other hand, starting with a highest possible copper valency of 2^+ charge balance would require holes on the oxygen sites as was experimentally found in Refs. [9] to [13].

In this paper we present an investigation of this question which to our knowledge for the first time is based on $O-K_z$ X-ray emission and $Cu-L_3$ X-ray self-absorption spectroscopy.

Since the copper valency or, alternatively, the number of holes on the oxygen sites depend on the oxygen content, we prepared samples with different oxygen contents ($6.0 < x < 6.9$). So we were able to look for differences between the signals from the superconducting sample ($x \approx 6.9$) with a formal copper valency of about 2.3 and the semiconducting samples with smaller oxygen content and therefore lower formal copper valencies.

Reprint requests to Prof. Dr. S. Steeb, Max-Planck-Institut für Metallforschung, Institut für Werkstoffwissenschaft, Seestraße 92, D-7000 Stuttgart 1.

2. X-Ray Self-Absorption Spectroscopy

In X-ray self-absorption spectroscopy the X-ray absorption coefficient $\mu(E)$ of an element is obtained with the help of two X-ray emission spectra generated with electrons of different energies E_1 and E_2 ($E_2 > E_1$) [14, 15]. The E_1-emission-spectrum is generated closer to the surface than the E_2-emission-spectrum. The intensities I_1 and I_2 of the measured emission spectra are given to a good approximation by

$$I_1 = I_{0,1} \cdot e^{-\mu(E) x_1} \tag{1}$$

and

$$I_2 = I_{0,2} \cdot e^{-\mu(E) x_2} \tag{2}$$

where $I_{0,1}$ and $I_{0,2}$ are the X-ray intensities at the point of X-ray generation inside the sample. x_1 and x_2 denote the mean pathlengths of the X-rays on their way inside the sample in direction to the X-ray spectrometer crystal. Dividing (1) by (2) yields an expression for $\mu(E)$:

$$\mu(E) = \frac{1}{x_2 - x_1} \left(\ln \frac{I_1}{I_2} - \ln \frac{I_{0,1}}{I_{0,2}} \right). \tag{3}$$

The intensities $I_{0,1}$ and $I_{0,2}$ depend on the current of the electron beam, the X-ray generation rates, the number of backscattered electrons, and the scattering of the primary electrons. These effects are dependent on the excitation conditions and have different influence on $I_{0,1}$ and $I_{0,2}$. On the other hand they do not depend on self-absorption. Therefore we compensate

0932-0784 / 89 / 0300-0180 $ 01.30/0. – Please order a reprint rather than making your own copy.

for them by fitting the E_2- to the E_1-emission spectrum in the energy region below the L_3-absorption edge (fitting region) by a two-parametrical fit, as already used in [16] for the evaluation of difference spectra:

$$I_{2,\mathrm{fit}} = \alpha I_2 + \beta. \tag{4}$$

The fit is done using $I_{2,\mathrm{fit}} \equiv I_1$ in the fitting region. The fitting parameter α deals with the effects mentioned above, whereas β accounts for the different background intensities of the E_1- and E_2-emission-spectra due to the energy-dependent position of the bremsberg and for the pre-edge absorption level.

Since all the differences between $I_{0,1}$ and $I_{0,2}$ are eliminated with the fitted E_2-spectrum ($I_{2,\mathrm{fit}}$), with $I_{0,1} = I_{0,2}$ we obtain from (3)

$$\mu_e(E) = \frac{1}{x_2 - x_1} \ln\left(\frac{I_1}{I_{2,\mathrm{fit}}}\right). \tag{5}$$

Here, $\mu_e(E)$ is the absorption coefficient with the pre-edge absorption level subtracted by the pre-edge fitting procedure.

In order to get an estimate for x_1 and x_2 we calculate the X-ray emission distribution curves according to [17] and [18]. We determine the mean x-positions by taking the x-values which divide the area under the distribution curves into two halves.

In the present paper we report on Cu–$L_{2,3}$ self-absorption spectra as obtained by recording Cu–$L_{\alpha,\beta}$ X-ray emission spectra of copper metal and various copper oxides. Since the intensities of the Cu self-absorption spectra as obtained with the various substances depend on the Cu concentration, they were normalized to the Cu self-absorption spectrum of elemental Cu. This was done using the equation,

$$\left(\frac{\mu}{\varrho}\right)_{\mathrm{compound}} = \sum_i g_i \left(\frac{\mu}{\varrho}\right)_i, \tag{6}$$

which describes the additivity of the mass absorption coefficients $(\mu/\varrho)_i$ of the elements i composing a substance. g_i is the mass fraction of element i.

With $\mu_{0,e}$ we will denote the mere height of the Cu edge-jump without considering its fine structure. Then (6) becomes

$$\left(\frac{\mu_{0,e}}{\varrho}\right)_{\mathrm{compound}} = g_{\mathrm{Cu}} \left(\frac{\mu_{0,e}}{\varrho}\right)_{\mathrm{Cu}}. \tag{7}$$

Introducing the normalization factor

$$F = \mu_{0,e,\mathrm{Cu}} / \mu_{0,e,\mathrm{compound}}, \tag{8}$$

(7) and (8) yield

$$F = \frac{1}{g_{\mathrm{Cu}}} \cdot \frac{\varrho_{\mathrm{Cu}}}{\varrho_{\mathrm{compound}}}. \tag{9}$$

3. Experimental

3.1. Electron Microprobe

The X-ray emission spectra were recorded with an electron microprobe (JEOL JXA-733) with two focusing linear spectrometers. The acceleration voltage of the electrons was set to 4 kV and 25 kV for the Cu–L- and to 10 kV for the O–K_α-spectra. The Cu–L radiation ($\lambda_{L_\alpha} = 13.336$ Å) was analyzed using a TAP crystal with resolution $\Delta\lambda/\lambda \approx 10^{-3}$. For the O–$K_\alpha$ radiation ($\lambda_{K_\alpha} = 23.62$ Å) we used a clinochlore crystal [19] with resolution better than $1.5 \cdot 10^{-3}$. Clinochlore has the advantage of not yielding the anomalous peak appearing with phtalate crystals [19, 20]. The spectrometer was calibrated with the Cu–L_α line of metallic Cu to be at 929.7 eV [21] and the O–K_α line of SiO_2 to be at 526.0 eV [22].

3.2. Sample Preparation

The $YBa_2Cu_3O_{6.9}$-samples were prepared from the starting materials Y_2O_3, BaO, and CuO, which were mixed in appropriate amounts with a tumbler for 2 hours and ground in an agate ball-mill to a mean particle size of 2 μm and sieved through a 100 mesh analytical sieve. Then the powder was calcined for 10 hours in air at 900 °C. After grinding and sieving again, the powder was calcined a second time under the same conditions, ground and sieved, and isostatically pressed into cylindrical pellets (630 MPa; 1 min.). The pellets were sintered in air for 1 h at 950 °C and then for 15 h at 900 °C with subsequent cooling to room-temperature with a cooling-rate of 1–2 K/min. The samples were cut into slices and annealed in flowing oxygen atmosphere for 65 hours at 400 °C. The characterization of the samples was done by standard four-point DC-resistivity measurements which yielded the superconducting transition temperature of 92 K and furthermore by X-ray diffraction, which showed the specimens to be single phase.

To establish the oxygen content of the $YBa_2Cu_3O_x$-samples, $YBa_2Cu_3O_{6.9}$-samples were heated at temperatures between 400 and 850 °C in a vacuum of 10^{-3} to 10^{-4} Torr within a quartz tube which was con-

Table 1. $YBa_2Cu_3O_x$-specimens. Oxygen content x and structure in dependence of the annealing temperature. o = orthorhombic; t = tetragonal.

Annealing Temp. [°C]	Oxygen content x in $Y_1Ba_2Cu_3O_x$	Structure
400	6.7	o
500	6.5	t
600	6.3	t
700	6.0	t
850	green phase	green phase

nected to the vacuum system. After 24 hours that part of the tube which contained the sample was melted away and rapidly quenched using liquid nitrogen. The oxygen contents related to the different annealing temperatures were determined by electron microprobe analysis. The results are shown in Table 1.

The structure of the samples was checked by X-ray diffraction. The non-annealed and the 400 °C-annealed sample show the orthorhombic structure, and the samples annealed at 500 to 700 °C show the tetragonal structure [23]. The structural phase transition between $x = 6.7$ and $x = 6.5$ is in accordance with the results of [23]. With the described vacuum annealing it was possible to adjust the oxygen contents at lower temperatures than in [24], where annealing was done in flowing atmosphere with various oxygen contents.

The $NaCuO_2$-sample was prepared by mixing and grinding Na_2O_2 and CuO in an agate-ball mill for 5 hours and heating the mixed powder for another 5 hours under oxygen atmosphere at 270 °C [25]. A Guinier diagram revealed that the major part of the specimen consists of $NaCuO_2$ besides CuO and negligible traces of NaCuO.

The $NaCuO_2$-powder as well as Cu_2O- (>97.0%; Fluka) and CuO-powder (>99.0%; Fluka) was pressed into pellets with a polished piston in order to get a very smooth surface.

4. Results and Discussion

4.1. O–K_α Spectra of La_2CuO_4 and $YBa_2Cu_3O_x$ ($6.0 < x < 6.9$)

In Fig. 1 we compare for La_2CuO_4 the measured O–K_α spectrum (++++) with the calculated local density spectra as obtained in [26] (full lines). O(1) labels the oxygen atoms within the CuO-planes which are part of the La_2CuO_4 perovskite structure and

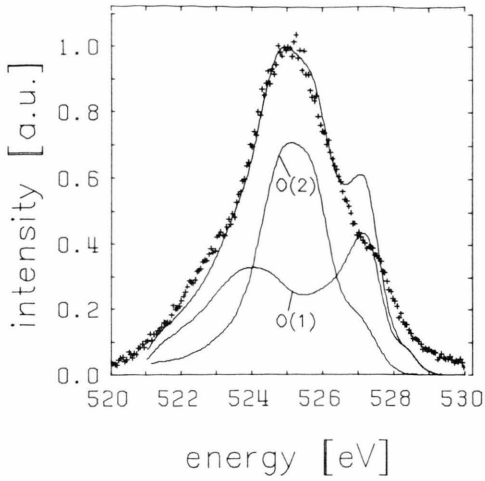

Fig. 1. La_2CuO_4; O–K_α spectrum; (++++) experimental values, (———) calculated spectra [26].

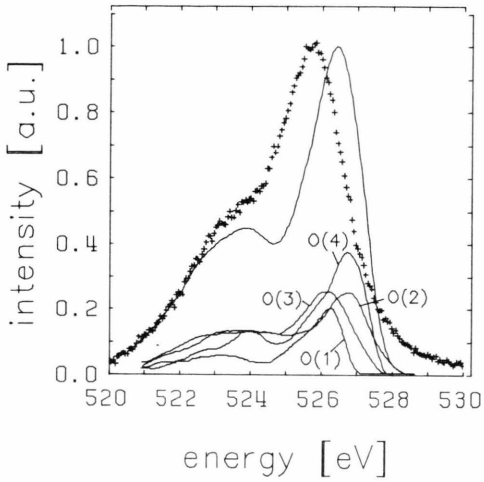

Fig. 2. $YBa_2Cu_3O_7$; O–K_α spectrum; (++++) experimental values, (———) calculated spectra [27].

O(2) the "out-of-plane" oxygen atoms. According to Fig. 1 the total calculated curve results from the sum of the partial curves. The calculated spectra from [26] were scaled with a reference energy E_0 which amounts in the presentation of Fig. 1 to 528.6 eV. E_0 at the same time means for the partial spectrum O(1) the Fermi energy. Except the peak at 527.1 eV the theoretical spectrum is in good agreement with the experimental run. Instead of that pronounced peak the experimental spectrum shows only a hump at 527.4 eV.

The spectrum obtained with $YBa_2Cu_3O_7$ is shown in Figure 2. Here for the calculated spectra [27] the

reference energy E_0 was set to 528.0 eV. Because of the different core-level binding energies only the Fermi-level of the O(2)-contribution coincides with E_0 [27]. O(2) and O(3) label the oxygen atoms in the CuO-planes, whereas O(1) and O(4) label those in the CuO-chains [28]. Both the experimental and the calculated $YBa_2Cu_3O_7$-spectra show essentially a two-peak structure, where the two peaks in the experimental spectrum are not fully resolved. This is due to the smaller peak separation in the experimental spectrum compared with the calculated one.

The slight misfit between calculated and experimental spectra in Figs. 1 and 2 arises because in the calculated spectra the two sub-peaks are more separated than in the experimental ones. According to [27] the calculated curve comes out too broad because the local density calculations assume metallic screening and therefore do not take into account the final state holes of the X-ray emission in the investigated compounds. These holes are much more localized in the upper π- or antibonding O–p states than in the lower bonding σ-states. Since localization involves less effective screening of the holes, a larger relaxation of the upper O–p states is expected. This in turn would result in a narrowing of the calculated spectra, which explains the difference between calculations and experiments.

At this point we stress the fact that, if besides O–2p final state holes which result from the X-ray emission there also would exist initial O–2p holes, the O–K_α spectra would be affected in a way comparable to that for final state O–p holes by hole-hole repulsion [27].

These considerations show that the deviations of the theoretical spectra from the experimental X-ray emission spectra is due to the same effect as the disagreement between the result of the local density calculations and the experimental photoelectron spectra as reported in [27].

Figure 3 shows O–K_α spectra of $YBa_2Cu_3O_x$ with variable oxygen content ($6.0 < x < 6.9$). The major change observed with decreasing oxygen content is the decrease of the main peak at 525.7 eV.

In Fig. 4 the difference spectra between the superconducting sample with $x = 6.9$ and the samples with lower oxygen content are shown. With decreasing oxygen content one would expect decreasing intensity of the emission spectrum and therefore a positive difference spectrum. The experimental difference curves in Fig. 4 correspond to this expectation in a general way. In the following we discuss slight deviations as observed mainly for the $x = 6.0$; 6.3; and 6.5-curves in the high energy region between 527 and 529 eV, where we observe negative difference-values. This is an indication for a broadening of the emission band with decreasing oxygen content. Referring to the previous discussion and neglecting the effect of the slight orthorhombic distortion in the superconducting compound, we attribute this broadening to a vanishing of initial-state holes in the O–2p states. Consequently,

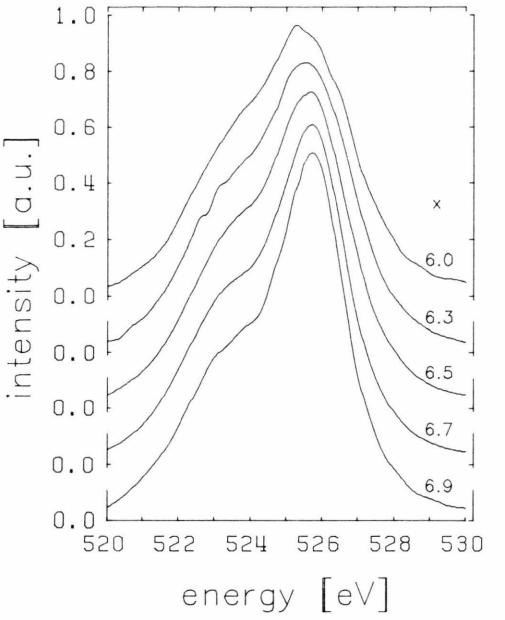

Fig. 3. $YBa_2Cu_3O_x$ with varying oxygen content x; O–K_α spectra.

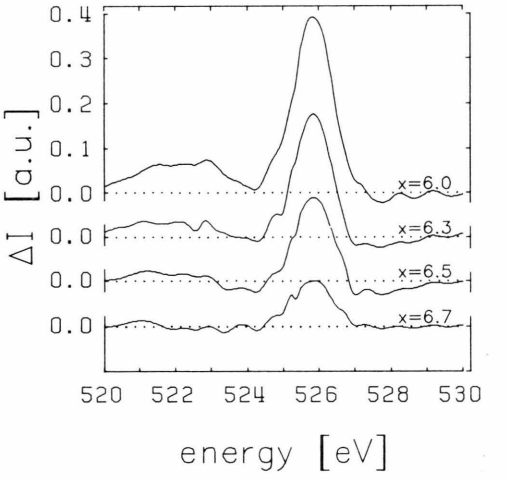

Fig. 4. $YBa_2Cu_3O_x$; ΔI = (Intensity $x = 6.9$) minus (Intensity $x = 6.0$; 6.3; 6.5; and 6.7).

this can be regarded as a proof for their existence in the superconducting compound $YBa_2Cu_3O_{6.9}$.

Now we will discuss the calculated partial spectra O(1) to O(4) as shown in Fig. 2 together with an experimental difference spectrum from Figure 4. All difference spectra roughly show the same shape. The difference curve with $x = 6.0$ would be most sensitive for the influence of oxygen. Since, however, this oxygen concentration is the limiting value for the existence of the phases under consideration in the present chapter (see Table 1) we choose the one with $x = 6.3$. Neglecting a change of the remaining Cu–O bonds with oxygen atoms removed, the difference curve with $x = 6.3$ stands for the signal from the 0.6 oxygen atoms per unit cell which make up the difference to the superconducting compound with $x = 6.9$. In Fig. 5 we compare that difference curve with each of the four calculated partial spectra, which are normalized to represent the contribution of one oxygen atom per unit cell.

Since the difference spectrum stands for the signal contribution of the removed oxygen atoms, the comparison in Fig. 5 can shed light on the question from which sites the oxygen atoms were removed during the heat treatment. By comparing not only the main maxima but furthermore the shape of the whole difference spectrum including the low energy tail, the best agreement between the experimental and calculated spectrum exists in the case of O(1) and maybe also of O(4), whereas in the cases of O(2) and O(3) the peak-to-tail ratio is too small. Therefore the removal of oxygen atoms from the positions O(2) and O(3), i.e. from the planes, can be excluded. It is not possible to decide further with the difference spectra, whether the O(1)- or the O(4)-atoms were removed. In [29] to [31] it was also found with neutron – and X-ray diffraction that the oxygen atoms are removed from the chains. Finally we want to draw attention to [23, 32] where the authors take into consideration that while one part of the O(4)-atoms is lost during the heat treatment the other part is redistributed in order to form a new set of Cu–O planes together with the O(1)-atoms.

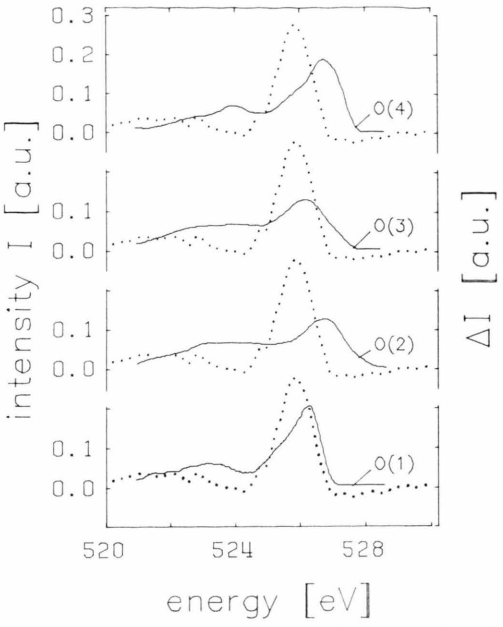

Fig. 5. $YBa_2Cu_3O_x$, $\Delta I|_{x=6.3}$ (·····) compared to the calculated [27] partial spectra O(1) to O(4) with intensity I (——).

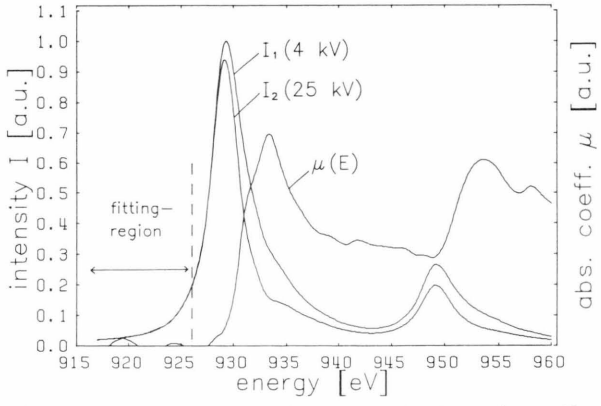

Fig. 6. $NaCuO_2$: Example for the evaluation of a self-absorption spectrum $\mu(E)$ from two emission spectra $I_1(E)$ and $I_2(E)$.

4.2. *Cu–$L_{2,3}$ Self-Absorption Spectra of $YBa_2Cu_3O_x$ ($6.0 < x < 6.9$) and other Copper Oxides*

In Fig. 6 we show two Cu–$L_{\alpha,\beta}$ emission spectra which were fitted according to the procedure described in section 2 and the resulting self-absorption spectrum $\mu(E) = \ln(I_1/I_2)$.

All self-absorption spectra shown in the present paper were evaluated from two emission spectra generated with 4 keV and 25 keV, respectively. Although the emission spectra were recorded with good counting statistics, they were smoothed with a cubic spline-fit before evaluating the self-absorption spectra. The position of the absorption edges was determined by their inflection points.

In the following we will compare Cu–$L_{2,3}$ self-absorption spectra of $YBa_2Cu_3O_x$ with variable oxy-

gen content with those of copper and different copper oxides, namely Cu_2O, CuO, and $NaCuO_2$. Figure 7 shows the corresponding spectra.

The self-absorption spectrum of metallic copper shows a step-like behaviour. Since the ground state of Cu is $3d^{10}4s^1$, the two steps represent the transitions from the spin-orbit split 2p-level ($2p_{1/2}$ and $2p_{2/3}$) to unoccupied 4s-states. The L_3-edge at 932.6 eV is due to transitions from the $2p_{3/2}$ core-level. The L_2-edge at 952.4 eV is due to transitions from the $2p_{1/2}$-core-level.

The self-absorption spectrum of Cu_2O shows humps at 935.1 and 954.1 eV. The shape of the Cu- and Cu_2O-spectra is in good agreement with the spectra obtained by thin film absorption in [33]. Expecting a filled 3d-shell ($3d^{10}$) with Cu_2O in the ground state, the absorption transitions to the 4s-states suggest the observed similarity of the Cu and Cu_2O self-absorption spectra.

A more dramatic change in the self-absorption spectra can be observed with the CuO-spectrum, which shows a remarkable shift of the edge position down to 930.3 eV due to a pronounced white line with a peak at 931.3 eV. The white line can be attributed to transitions from the $2p3d^9$-ground state to a $\underline{2p}3d^{10}$-final state (underlining means hole state). The CuO self-absorption spectrum is in good accordance with [33] and with electron-energy-loss-studies in [34]. At this point we mention the white lines as observed in [35] in the total electron yield spectrum of Cu_2O, which are much more pronounced than the weak indications as observed with self-absorption in the present Figure 7.

The ground state of possible trivalent copper in $NaCuO_2$ is $3d^8$. However, because of the covalent character of the Cu3d-O2p-bonds, and since copper rather can be found in the divalent or monovalent state, $3d^9\underline{L}$ and $3d^{10}\underline{L}^2$ ground states can be expected. $\underline{L}$ stands for a hole in the oxygen ligand. Van der Laan et al. [36] expect the $\underline{2p}3d^9$ final state to be several eV above $\underline{2p}3d^{10}\underline{L}$ due to the Coulomb interaction of the 2p core hole with the 3d electrons. Therefore the white line peaks at 933.4 and 953.6 eV are assigned to $\underline{2p}3d^{10}\underline{L}$ final states. These peak positions are in good accordance with the results in [13]. The shoulder at 931.3 eV on the low energy flank of the white line arises from the white line of the CuO-impurities, which could be identified using X-ray diffraction according to the Guinier-method. The edge position of the $NaCuO_2$ self-absorption spectrum with the white

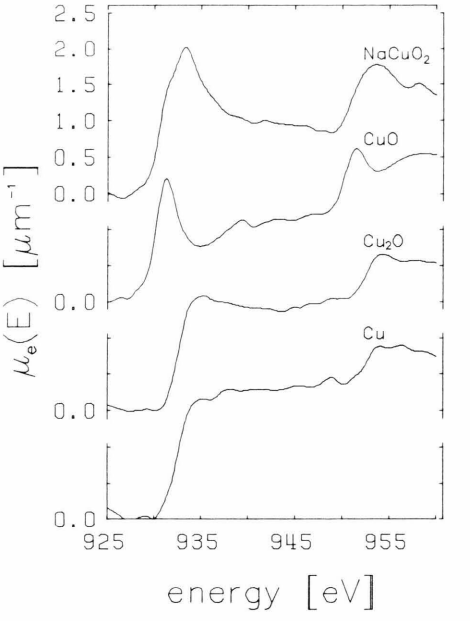

Fig. 7. Cu–$L_{2,3}$ self-absorption spectra of Cu, Cu_2O, CuO, and $NaCuO_2$.

line of CuO removed turns out to be at 932.3 eV (see Figure 9a). Thereby the best fit of the CuO white line was obtained using a 50% mixture of a Gaussian and a Lorentzian lineshape.

In Fig. 8 the self-absorption spectra of $YBa_2Cu_3O_x$ ($6.0 < x < 6.9$) are shown in the region of the L_3 white lines. Since the data for the energy-range above the L_z-peak (including the less intense L_β-peak) are of lower precision because of the low emission intensity, we restrict our further observations to the region of the L_3 white line. This is reasonable, too, because of the low copper concentration in $YBa_2Cu_3O_x$ and the small effects we are expecting.

It can be seen that the width of the white line increases with increasing x and that its peak position is shifted to higher energies. For comparison the spectrum of CuO is included (dashed spectrum) and its peak position marked with the vertical dashed line. Since the white lines for $x = 6.5$ and $x = 6.3$ show the same position and width as the one for CuO, we conclude that in these samples divalent copper with the $3d^9$-ground state ($\underline{2p}3d^{10}$ final state) is dominant. For the sample with $x = 6.0$ the intensity of the white line has decreased, which is a sign of a decreasing $3d^9$-ground state contribution. Removing the white line (see Fig. 9b) shifts the absorption edge to 932.9 eV,

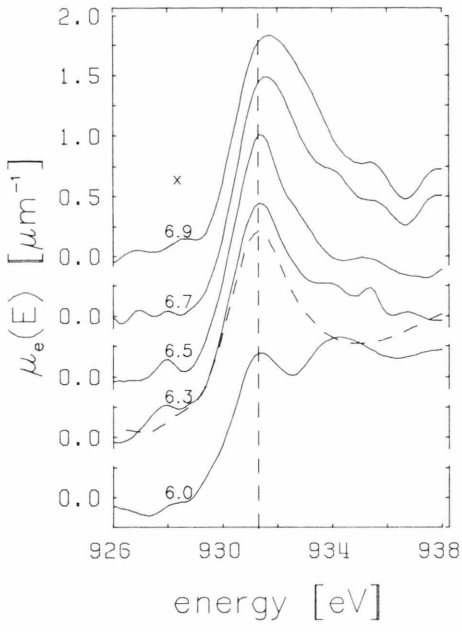

Fig. 8. $YBa_2Cu_3O_x (6.0 < x < 6.9)$; $Cu-L_3$ self-absorption spectra. (– – –) $Cu-L_3$ self-absorption spectrum of CuO.

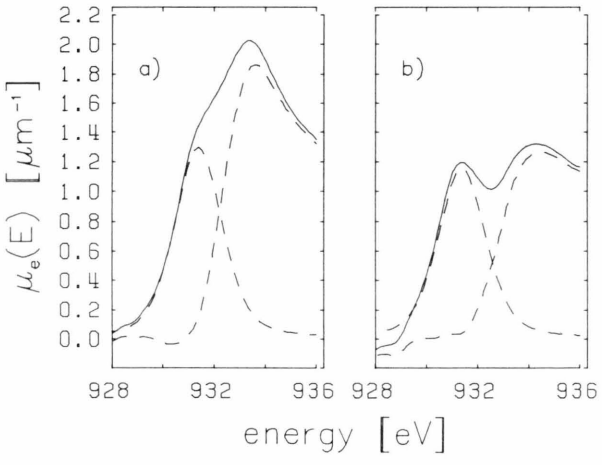

Fig. 9. $Cu-L_3$ self-absorption spectra with separated $2p3d^{10}$ final state white line. a) $NaCuO_2$, b) $YBa_2Cu_3O_{6.0}$.

which is close to that one of the Cu_2O-spectrum. The resemblance between the spectrum with the white line removed and the Cu_2O-spectrum strongly suggests the presence of monovalent copper, as can be expected for this compound with its low oxygen concentration.

The broad white lines of the two upper spectra in Fig. 8 arise from the contribution of the $3d^9\underline{L}$-ground state ($\underline{2p}3d^{10}\underline{L}$-final state) at about 933.4 eV as already observed in the spectrum of $NaCuO_2$. Its presence is strongest in the superconducting sample with $x = 6.9$. This observation is in good agreement with our results from the $O-K_\alpha$ emission spectra, where we also deduced ground-state holes in the O–2p band in the superconducting sample. The decrease of the contribution at 933.4 eV with decreasing oxygen content is a confirmation of the results in [37], where the $Cu-L_3$ electron-yield spectrum of a superconducting sample is compared to the one of a sample with a somewhat smaller oxygen content.

4.3. The Green Phase Y_2BaCuO_5

In this section we will present the spectra obtained for the non-superconducting insulating phase Y_2BaCuO_5, also called the green phase.

The $Cu-L_3$ self-absorption spectrum (Fig. 10) shows a sharp white line at 931.0 eV. At energies above the white line the self-absorption drops to zero and then a small peak shows up at 935.7 eV. At 937.2 eV the absorption edge of a small band of unoccupied states arises.

The white line of Y_2BaCuO_5 is sharper than the one of CuO (dashed spectrum in Fig. 10) and shifted by about 0.3 eV to lower energies. According to [33] this behaviour reveals the ionic character of the green phase. The white line arises from highly localized $\underline{2p}3d^{10}$ final states lying within the energy gap of the insulating compound. We contribute the small peak at 935.7 eV to excitons where the screened core hole and the ejected electron form hydrogenlike bound states. The difference between the position of the absorption edge at 937.2 eV and the L_α emission peak of the 4 kV emission spectrum is 7.6 eV. Since the peak of the L_α emission line is about 2 to 3 eV below the valence band edge, 5 eV seems to be a good estimate of the energy-gap. In Fig. 10 the gap region is marked with an arrow.

In the following we will discuss the $O-K_\alpha$ emission spectrum for the green phase (Fig. 11). Whereas the $O-K_\alpha$ spectrum of the superconducting compound (dashed line in Fig. 11) shows its main peak on the high-energy side of the emission band, the one of the green phase is located on the low-energy side. Considering the shoulders on the opposite sides it can be seen that the two spectra show some mutual symmetry with respect to the energy of 525.3 eV.

In [38] the $O-K_\alpha$ spectra of various substances are divided into two groups depending whether the main

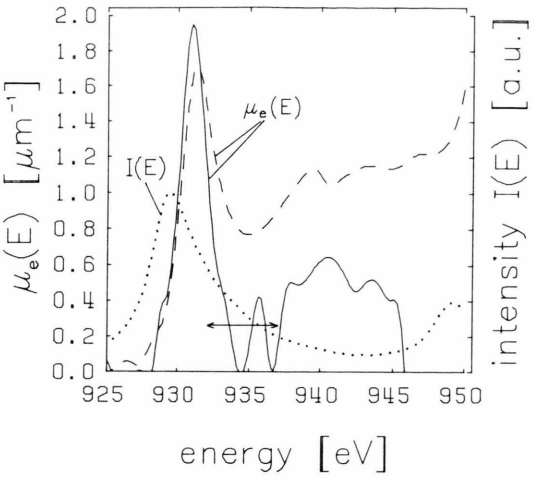

Fig. 10. Cu–L_3 self-absorption spectra and emission spectrum: (———) Y_2BaCuO_5; Cu–L_3 self-absorption spectrum, (– – –) CuO; Cu–L_3 self-absorption spectrum, (···) $Y_2BaCu_3O_5$; Cu–L_α emission spectrum.

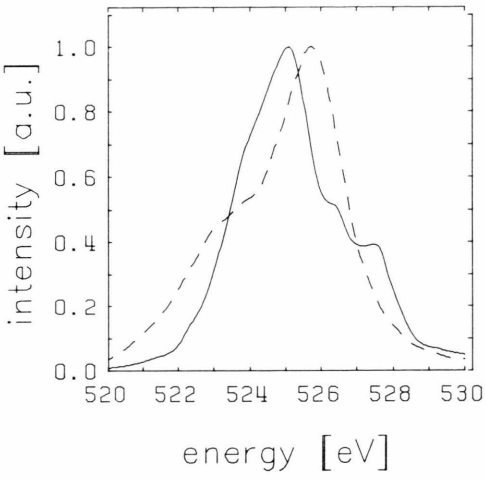

Fig. 11. O–K_α emission spectrum. (———) Y_2BaCuO_5 (green phase), (– – –) $YBa_2Cu_3O_{6.9}$ (superconducting phase).

peak is located in the low- or the high-energy region of the emission band. The compounds belonging to the first group are oxides of elements with lower electronegativity than those of the second group. Therefore the bonding in the oxides of the first group is more polar than in those of the second group. Since the O–K_α spectrum of the green phase with its dominant peak in the low-energy region can be attributed to the first group, the ionic character of its Cu–O bonds is also confirmed with the O–K_α spectrum. On the other hand, the peak on the high-energy side of the $YBa_2Cu_3O_{6.9}$-spectrum is in accordance with the covalent character of the superconducting compound.

Acknowledgements

We would like to thank Ch. Rossel and J. G. Bednorz from the IBM Research Laboratory Zürich for supplying us with the La_2CuO_4-sample.

[1] J. G. Bednorz and K. A. Müller, Z. Phys. B **64,** 189 (1986).
[2] C. W. Chu, P. H. Hor, R. L. Meng, L. Gao, Z. J. Huang, and Y. Q. Wang, Phys. Rev. Lett. **58,** 405 (1987).
[3] M. K. Wu, J. R. Ashburn, C. J. Torng, P. H. Hor, R. L. Meng, L. Goa, Z. J. Huang, Y. Q. Wang, and C. W. Chu, Phys. Rev. Lett. **58,** 908 (1987).
[4] E. E. Alp, G. K. Shenoy, D. G. Hinks, D. W. Capone II, L. Soderholm, H.-B. Schuttler, J. Guo, D. E. Ellis, P. A. Montano, and M. Ramanathan, Phys. Rev. B. **35,** 7199 (1987).
[5] G. M. Antonini, C. Calandra, F. Corni, F. C. Matacotta, and M. Sacchi, Europhys. Lett. **4,** 851 (1987).
[6] H. Eickenbusch, W. Paulus, R. Schöllhorn, and R. Schlögl, Mat. Res. Bull. **22,** 1505 (1987).
[7] F. W. Lytle, R. B. Greegor, and A. J. Panson, Phys. Rev. B **37,** 1550 (1988).
[8] W. Herzog, M. Schwarz, H. Sixl, and R. Hoppe, Z. Phys. B **71,** 19 (1988).
[9] A. Bianconi, A. Congiu Castellano, M. De Santis, P. Delogu, A. Gargano, and R. Giorgi, Sol. State Comm. **63,** 1135 (1987).
[10] A. Fujimori, E. Takayama-Muromachi, and Y. Uchida, Sol. State Comm. **63,** 857 (1987).
[11] S. Horn, J. Cai, S. A. Shaheen, Y. Jeon, M. Croft, C. L. Chang, and M. L. den Boer, Phys. Rev. B **36,** 3895 (1987).
[12] P. Steiner, S. Hüfner, V. Kinsinger, I. Sander, B. Siegwart, H. Schmitt, R. Schulz, S. Junk, G. Schwitzgebel, A. Gold, C. Politis, H. P. Müller, R. Hoppe, S. Kemmler-Sack, and C. Kunz, Z. Phys. B **69,** 449 (1988).
[13] D. D. Sarma, O. Strebel, C. T. Simmons, U. Neukirch, G. Kaindl, R. Hoppe, and H. P. Müller, Phys. Rev. B **37,** 9784 (1988).
[14] R. J Liefeld in: D. J. Fabian (ed.), Soft X-Ray Band Spectra, Acad. Press, London, New York 1968, p. 133.
[15] S. Hanzely and R. J. Liefeld in: Bernett (ed.), Electronic Density of States, NBS spec. publ. No. 323 (1971).
[16] S. El-Kholy and K. Ulmer, Z. Phys. B **38,** 1 (1980).
[17] A. R. Büchner and W. Pitsch. Z. Metallkunde **62,** 392 (1971).
[18] A. R. Büchner and W. Pitsch, Z. Metallkunde **63,** 398 (1972).

[19] W. L. Baun and E. W. White, Anal. Chem. **41,** 831 (1969).
[20] D. G. W. Smith, R. K. O'Nions, and K. Norrish, Spectroch. Acta **29 B,** 63 (1974).
[21] International Tables for X-Ray Crystallography, Vol. IV, Kynoch Press, Birmingham 1974.
[22] T. L. Gilbert, W. J. Stevens, H. Schrenk, M. Yoshimine, and P. S. Bagus, Phys. Rev. B **8,** 5977 (1973).
[23] P. K. Gallagher, H. M. O'Bryan, S. A. Sunshine, and D. W. Murphy, Mat. Res. Bull. **22,** 995 (1987).
[24] P. K. Gallagher, Adv. Ceramic Mat. **2** (No. 3 B, Special Issue), 632 (1987).
[25] K. Hestermann and R. Hoppe, Z. Anorg. Allg. Chem. **367,** 261 (1969).
[26] J. Redinger, J. Yu, A. J. Freeman, and P. Weinberger, Phys. Lett. A **124,** 463 (1987).
[27] J. Redinger, A. J. Freeman, and S. Massidda, Phys. Lett. A **124,** 469 (1987)
[28] S. Massidda, J. Yu, A. J. Freeman, and D. D. Koelling, Phys. Lett. A **122,** 198 (1987).
[29] P. Bordet, C. Chaillout, J. J. Capponi, J. Chenavas, and M. Marezio, Nature **327,** 687 (1987).
[30] J. van den Berg, C. J. van der Beek, P. H. Kes, G. F. Nieuwenhuys, J. A. Mydosh, H. W. Zandbergen, F. P. F. van Berkel, R. Steens, and D. J. W. Ijdo, Europhys. Lett. **4,** 737 (1987).
[31] W. K. Kwok, G. W. Crabtree, A. Umezawa, B. W. Veal, J. O. Jorgensen, S. K. Malik, L. J. Nowicki, A. P. Paulikas, and L. Nunez, Phys. Rev. B **37,** 106 (1988).
[32] W. K. Ford, C. T. Chen, J. Anderson, J. Kwo, S. H. Liou, M. Hong, G. V. Rubenacker, and J. E. Drumheller, Phys. Rev. B **37,** 7924 (1988).
[33] A. S. Koster, Mol. Phys. **26,** 625 (1973).
[34] R. D. Leapman, L. A. Grunes, and P. L. Fejes, Phys. Rev. B **26,** 614 (1982).
[35] S. L. Hulbert, B. A. Bunker, F. C. Brown, and P. Pianetta, Phys. Rev. B **30,** 2120 (1984).
[36] G. van der Laan, C. Westra, C. Haas, and G. A. Sawatzky, Phys. Rev. B **23,** 4369 (1981).
[37] A. Bianconi, A. Congiu Castellano, M. De Santis, P. Rudolf, P. Lagarde, A. M. Flank, and A. Marcelli, Sol. State Comm. **63,** 1009 (1987).
[38] H. M. O'Bryan and H. W. B. Skinner, Proc. Roy. Soc., London **A176,** 229 (1940).